References

[1] Lin, Y. K., *Probabilistic Theory of Structural Dynamics*, McGraw-Hill, New York, 1967.

[2] Corcos, G. M. and Liepman, H. W., "On the Contribution of Turbulent Boundary Layer to the Noise Inside a Fuselage," TM 1420, 1956, NACA.

[3] Ribner, H. R., "Boundary Layer Induced Noise in the Interior of Aircraft," U.T.I.A. Rept. 37, 1956, Univ. of Toronto, Toronto, Canada.

[4] Kraichnan, R. H., "Noise Transmission from Boundary Layer Pressure Fluctuations," *Journal of the Acoustical Society of America*, Vol. 29, 1957, pp. 65–71.

[5] Dyer, I., "Response of Plates to Decaying and Convecting Random Pressure Field," *Journal of the Accoustical Society of America*, Vol. 31, 1959, pp. 922–928.

[6] Lin, Y. K., "Stresses in Continuous Skin-Stiffened Panels Under Random Loading," *Journal of the Aerospace Sciences*, Vol. 29, 1962, pp. 67–75.

[7] Brillouin, L., *Wave Propagation in Periodic Structures*, Dover, New York, 1953.

[8] Miles, J. W., "Vibrations of Beams on Many Supports," *Journal of Engineering Mechanics Division*, ASCE, Vol. 82, (EMI), Jan. 1956, pp. 1–9.

[9] Lin, Y. K., "Free Vibration of Continuous Skin-Stringer Panels," *Journal of Applied Mechanics*, Vol. 27, Dec. 1960, pp. 669–676.

[10] Lin, Y. K., "Free Vibration of Continuous Beams on Elastic Supports," *International Journal of Mechanical Sciences*, Vol. 4, Oct. 1962, pp. 409–423.

[11] Lin, Y. K., Brown, I. D., and Deutschle, P. C., "Free Vibrations of a Finite Row of Continuous Skin-Stringer Panels," *Journal of Sound and Vibration*, Vol. 1, Jan. 1964, pp. 14–27.

[12] Lin, Y. K. and McDaniel, T. J., "Dynamics of Beam Type Periodic Structures," *Transactions of the ASME: Journal of Engineering for Industry*, Vol. 91, Nov. 1969, pp. 113–1141.

[13] Mead, D. J. and Pujara, K. K., "Space-harmonic Analysis of Periodically Supported Beams; Response to Convected Random Loading," 1970, Inst. of Sound and Vibration Research, Univ. of Southampton, England.

[14] Mead, D. J., "Vibration Response and Wave Propagation in Periodic Structures," Paper 70-WA/DE-3, Jan. 1971, ASME.

[15] Pestel, E. C. and Leckie, F. A., *Matrix Methods in Elastomechanics*, McGraw-Hill, New York, 1963.

[16] Lin, Y. K. and Donaldson, B. K., "A Brief Survey of Transfer Matrix Techniques with Special Reference to the Analysis of Aircraft Panels," *Journal of Sound and Vibration*, Vol. 10, Jan. 1969, pp. 103–143.

Supersonic Flow over Convex and Concave Shapes with Radiation and Ablation Effects

IHOR O. BOHACHEVSKY* AND RONALD N. KOSTOFF †

Bellcomm Inc., Washington, D.C.

A first-order accurate numerical method of unsteady adjustment is employed to calculate inviscid flowfields about convex and concave shapes. Two geometries are used: 1) conical forebodies with spherical afterbodies whose cone half-angles range from 50° to 135° and 2) thin-walled cylinders with cylindrical cavities of different depth facing the oncoming stream. Computations with radiative heat-transfer effects are carried out for flows over 50.56° and 79.83° half-angle cones. A gray gas model is assumed; no restriction is placed on the optical thickness nor is a slab approximation made. Results show a significant departure from the slab approximation near surface discontinuities and large radiative energy losses near cold surfaces. Flows over concave shapes, i.e., the 120° and 135° cones and the two cylinders, relax to their steady-states in a damped oscillatory manner. Higher-order accurate computations are necessary to resolve the nature of these oscillations.

I. Introduction

KNOWLEDGE of the flowfield about a spacecraft entering an atmosphere is important in vehicle design and mission planning. For example, the flowfield determines the dependence of aerodynamic loads and heat-transfer rates (both convective and radiative) on entry trajectory; specification of the charged particle concentration within the flowfield delineates that portion of the entry path where communication blackout occurs. Also, familiarity with the flow pattern assists experimenters in the selection of the most favorable locations on the vehicle surface for placement of their instruments.

Extensive and successful studies of flowfields associated with atmospheric entry vehicles have been performed in the past; the literature pertaining to these investigations is too vast to be discussed here. It is known that, depending on the forebody geometry and the freestream conditions, either of two cases occurs: the shock wave is attached with a supersonic flow behind it, or the shock wave is detached with a mixed subsonic-supersonic flow behind it.

These two cases have always been investigated separately; to the best of our knowledge no method for determining the flowfield exists that does not require prior knowledge of the nature of bow shock configuration. However, as planning and technology become more refined, it becomes desirable to perform flowfield computations for a portion of the trajectory along which the shock configuration changes from attached to detached. Such change of configuration may be caused by the change of freestream conditions or by large ablation rates and excessive blunting of the tip due to erosion.

Recent planning of future space missions envisages extensive use of mass injection from the forebody of the vehicle into the flowfield. This may be either for cooling[1] or, through the application of retrorockets, for assisting in the aerodynamic braking during atmospheric entry.[2] Effective exploitation of these devices

Presented as Paper 71-55 at the AIAA 9th Aerospace Sciences Meeting, New York, January 25–27, 1971; submitted November 3, 1971; revision received February 25, 1972. This work was supported by NASA OMSF under Contract NASW-417.

Index categories: Hypersonic Flows; Radiating Flows; Nonsteady Aerodynamics.

* Member, Technical Staff. Member AIAA.

† Member, Technical Staff.

and related ideas will depend on understanding of the flowfields and the ability to determine these for all entry conditions.

A numerical approach to computation of flowfields for engineering applications should be both relatively accurate and conceptually simple. It should also be sufficiently general to be applicable to flows with large surface mass injection and radiative heat transfer as well as to asymmetric flows corresponding to vehicles at nonzero angles of attack. Finally, it should be easy to modify in case the need for an improvement in accuracy and/or resolution becomes evident in applications to problems where accuracy is crucial, i.e., shock-on-shock interactions or oscillating shock problems.

The purpose of the present paper is to describe a method meeting the aforementioned requirements and to present some results obtained with it. The paper is organized as follows: the mathematical problem is posed in Sec. II and the numerical procedure used to solve it is presented in Sec. III. The treatment of radiation phenomena is described in Sec. IV and the results are presented in Sec. V. The final section summarizes the work and indicates some possible future developments and applications.

The method depends in part on the family of shapes to be examined. In the present study these are: 1) finite length cone with spherical afterbody and 2) hollow cylinder. The conical shape is popular in engineering design and allows representation of major classes of different flowfields with the variation of a single parameter, the cone half-angle, in the range from 0° to 180°. This range covers the small angle case of attached bow shock (Fig. 1A), the medium angle case of detached bow shock (Fig. 1B), and the large angle case where oscillating bow shocks may occur (Fig. 1C). The hollow cylinder is convenient for the study of oscilatory flow phenomena.

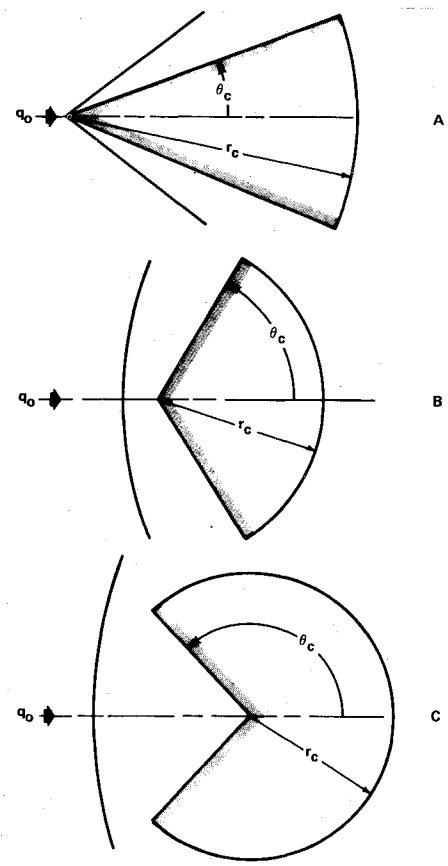

Fig. 1 Shock configuration for different cone angles.

II. Formulation of the Problem

A. General Approach

To determine the steady flowfield about a prescribed body shape it is necessary to solve the conservation equations of gas dynamics for a given gas model and with appropriate boundary conditions. When an inviscid flowfield contains detached shocks, the steady-state equations are hyperbolic in the supersonic region and elliptic in the subsonic region leading to a mixed problem for which the solution is exceedingly difficult and complex. In the present investigation the treatment is based on the unsteady approach in which the time dependent form of the conservation equations is solved and the desired steady-state solution is that which obtains after a long period of time, i.e., the large-time asymptote. The unsteady form of conservation equations is everywhere hyperbolic; thus the problem has been converted from a mixed hyperbolic-elliptic free boundary value problem to a hyperbolic initial-boundary value problem which is mathematically more tractable. This approach has been applied successfully to aerodynamical problems by several investigators.[3-7]

B. Coordinate System and Differential Equations

To simplify the application of the boundary conditions, it is convenient in general to employ a coordinate system with coordinate surfaces that coincide with the given boundaries. For computation of flows over cones with spherical afterbodies, it is natural to use a spherical polar coordinate system as shown in Fig. 2, where r is the distance from the origin and θ and ϕ are the two angular coordinates. The cone axis is directed along the line $\theta = 0$ and its vertex is located at $r = 0$. $\theta = \theta_c$ = const represents the cone surface while $r = r_c$ = const represents the spherical afterbody surface. For symmetric flows in the absence of radiation ϕ is an ignorable coordinate; when radiative effects are introduced in Sec. IV, ϕ will be taken into account.

In the investigation of flows over cylinders it is convenient to use cylindrical coordinates with x denoting the distance along the axis, y the radius normal to the cylinder axis, and ϕ the azimuthal coordinate; for symmetric flows ϕ again is ignorable.

The conservation forms of the differential equations that govern the flow of an ideal, inviscid gas in spherical and cylindrical coordinates are well known and need not be included here. These equations are listed and discussed, for example, in Refs. 3, 4, and 8; the last reference also contains all details of the analysis and computations reported in this paper.

C. Boundary Conditions

The complete formulation of the problem must include suitable boundary conditions; in the present case these are standard.

At the solid surfaces of the body, the boundary condition should require only the vanishing of the normal velocity component. At the outer edge of the field, upstream of the nose, the solution must assume the prescribed freestream values. Downstream of the nose section, the flow variables should tend to approximately constant values along the individual streamlines. Along the axis, the usual symmetry conditions apply.

Special considerations are required at the origin, $r = 0$, because it is the singular point of the spherical coordinate system. This singularity differs from the singularity on the axis that is usually eliminated by a limiting process. At the present time, only the regularity of the solution at $r = 0$ will be required. The way this condition is enforced will be discussed in a later section. Similar statements apply to the sharp intersection between the cone surface and the spherical afterbody; the treatment of this locus will be described later.

For the present problem, in which the steady-state solution is of prime interest, initial conditions could, in principle, be prescribed arbitrarily. A straightforward procedure is to accelerate the body impulsively to the freestream velocity; freestream values are thus specified as initial conditions everywhere in the field. Alternate ways of prescribing the initial conditions will be mentioned later.

D. Thermodynamic Gas Model

To form a closed system, the conservation equations must be supplemented with a thermodynamic relation between the state

variables density ρ, pressure p, and enthalpy h. For an ideal gas, which is considered here, this relation is

$$h = [\gamma/(\gamma-1)]p/\rho$$

In general, γ the ratio of specific heats, is not a constant, but a function of temperature and density. However, Ref. 9 shows that an "effective" γ may be obtained by approximating the empirical relationship between h and p/ρ with a straight line. In the present computations $\gamma = 1.4$ is used for moderate Mach numbers and $\gamma = 1.2$ for hypersonic Mach numbers when the effect of radiation is taken into account.

III. Numerical Procedure

A. Background

The differencing scheme used in our computations is an adaptation of the one originally proposed by P. D. Lax.[10] It is the simplest technique available[3,4] and easy to modify. As Richtmyer and Morton have observed,[11] successive repetition of computational steps in Lax's scheme with only minor modifications (the two-step method) results in an equivalent to the second-order accurate Lax-Wendroff scheme.[12] A further increase in accuracy, to third order, is also possible by the addition of a moderately complicated third iteration; the final result becomes equivalent to the scheme devised recently by Rusanov.[13]

B. Computational Mesh and Finite-Difference Equations

The mesh employed in finite-difference computations of flows over cones is similar to the grid used on commonly available polar-coordinate graph paper in which new angular divisions, $\Delta\theta$, are added as the distance from the origin increases so that the linear mesh dimensions remain nearly constant in all sections of the grid. This is necessary to obtain equal resolution in all parts of the field. Computations with a varying linear mesh size (constant angular steps) resulted in unequal resolution in different regions because the maximum time step is governed by the smallest linear mesh dimension. In practice, whenever $r\Delta\theta$ doubles, the value of $\Delta\theta$ is halved. Thus the product $r\Delta\theta$ is kept approximately equal to the radial increment Δr. The arcs along which new angular divisions are added are called internal boundaries. For computations in cylindrical coordinates a rectangular grid with $\Delta x = \Delta y = 1$ cm was used.

On the computational grids just specified, the differential form of the conservation equations is approximated by replacing time derivatives by first forward differences and space derivatives by first central differences. The first-order accurate scheme thus obtained is known to be unconditionally unstable and to stabilize it, a second-order dissipative term in the form of a Laplacian of the conservation variable is added.[10,3,4] The explicit expressions used in calculations are listed in Appendix I of Ref. 8.

C. Boundary Conditions for the Difference Equations

Because central differences and higher-order dissipative terms are used that necessitate specification of variables at points exterior to the computational mesh when advancing boundary points with time, boundary conditions additional to those stated in Sec. II.C are required. There is no a priori physical basis for their specification; these conditions can be justified only a posteriori by the results.

At the solid boundaries the first derivatives normal to the surface of all flow variables, with the exception of the normal velocity component, are set equal to zero. The normal velocity component is extrapolated through zero at the surface; this appears to be a good approximation for flows with small gradients near the wall and it automatically satisfies the normal momentum equation at the surface. For flows with large vorticity, such as those including surface mass injection, the pressure at the auxiliary point is specified in such a way that the normal momentum equation at the surface is satisfied with the prescribed value of mass addition from the surface.

Corner points are treated as triple valued; values there are advanced as if they were not on the boundary but in the flowfield. This implies a slight rounding of the corner. However, when the boundary points adjacent to the corner are advanced, they each regard it as a point on their respective boundary. Handling the singularity in this fashion correctly locates the sonic line at the corner and helps to control the local expansion gradients; it constitutes an improvement over the treatment accorded to this point in Refs. 3 and 4.

The auxiliary points at the upstream outer boundary are assigned freestream values throughout the computation. At the downstream end of the mesh the flow variables are extrapolated linearly to the exterior points. At the internal boundaries, (arcs across which the size of $\Delta\theta$ changes) the values at nonmesh points on arcs $r-\Delta r$ are obtained from a linear interpolation between the values at the two adjacent points on that arc. On the axis of symmetry of the flow the reflection condition is used.[3]

The cone vertex, $r = 0$, is a singular point in the field and an improper treatment of it will greatly distort the flowfield.[14] The spherical form of the difference equations, however is not dependent on the manner in which values at the vertex are specified because the coefficients of those values vanish at the origin. For purposes of the presentation of results which include the vertex, this point is treated as a multivalued one and quantities there are obtained by extrapolation along radial lines to the vertex.

The initial state of the field may be specified arbitrarily; it is simplest to begin the computations from the prescription of freestream values everywhere, as stated in Sec. II.C. For many purposes, however, it is convenient to store the results of one computation on a magnetic tape and use them as initial conditions for new calculations. In this way, computer time is saved when solving a series of problems or investigating parametric dependence.

After the field is initialized the boundary conditions are applied to initialize the region exterior to the field. The finite difference equations are then used to advance the variables from their values at $t = 0$ to values at $t = \Delta t$ and the process is repeated until the steady-state or periodic behavior is attained.

To assure stability of the computation, the time increment Δt used must be that which is given approximately by the Courant-Friedrichs-Lewy condition[3,15] which requires that numerical propagation speed be not less than the fastest physical propagation speed. In practice the maximum Δt which can be used consistent with stable computations is determined by experimentation to be within approximately 20% of the value given by the C-F-L condition. It is desirable to use the largest possible Δt in order to minimize the smearing of the shocks.

IV. Radiation Effects

For high-velocity flight, e.g., superorbital entry conditions, a satisfactory description of the flowfield should include the effects of radiative heat transfer. Two major difficulties arise in the treatment of this phenomenon: the variation of the absorption and emission coefficients with frequency and the three-dimensional nature of the radiation field.

In the present paper, we concentrate on the geometrical aspect of the problem for the flow over a cone; i.e., the determination of radiative contribution from 4π steradians without any restrictive assumptions on the symmetry properties of the radiating field or optical thickness of the medium. Previous calculations of radiation phenomena were concerned mainly with the construction of band absorption models for the treatment of frequency dependence. The literature pertaining to this topic is too rich to be discussed here; a review is given in a recent survey article by Anderson.[16] In these investigations of spectral effects the assumption of slab symmetry has always been made. This simplification, however, is not justified for a sharp cone because the tangent plane is a poor approximation to the cone surface near the vertex.

The conditions for which energy transported by radiation is significant and the integral expressions that describe this transport may be found in Ref. 8 together with the computational details. Here we will only indicate the technique used to compute

the radiative contribution to the energy balance; it makes essential use of transformation formulae between two spherical coordinate systems.

To evaluate the radiative energy transport we introduce at each mesh point of the flowfield a local spherical coordinate system, as shown in Fig. 2, where ψ is the angle measured from the extension of the radius r, λ is the azimuth angle around r, and R is the distance along the ray (ψ, λ). At each point (θ_i, r_j) we select a set of pairs (ψ_n, λ_m) and check each ray (ψ_n, λ_m) for the intersection with the solid surface of the cone; if the ray intersects the cone, we compute the distance R_s at which that happens. We then step off along the ray with intervals of length dR and determine the θ, r, and ϕ coordinates at the endpoint of each interval from the coordinate transformation formulas.[8] After elimination of the ignorable coordinate ϕ, we determine from these coordinates, by a double interpolation procedure, the thermodynamic state of the medium for each point on the ray. With this information it is easy to sum over the necessary dR intervals and obtain the optical thickness τ, calculate the corresponding absorption, and sum again to obtain the contribution from the entire ray. A subsequent double summation over n and m, with appropriate differentials $d\psi$ and $d\lambda$, that covers the unit sphere completes the computation of radiative energy contribution in each frequency band. By combining the amounts of energy added in each considered frequency range, we obtain the total energy delivered by the radiation transport.

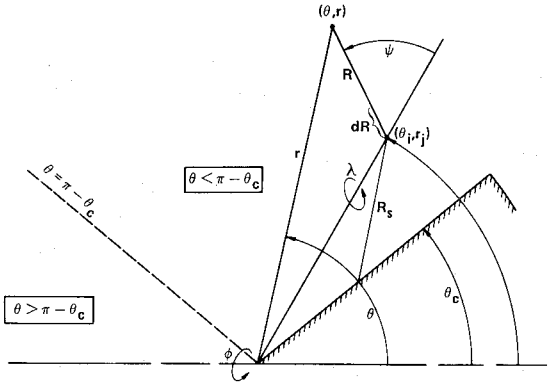

Fig. 2 Spherical coordinate systems.

V. Numerical Results

We will now present typical results obtained with the previously described method. These results were selected to illustrate the three novel aspects of our work: A) applicability to attached and detached shock wave configurations, B) absence of slab approximation or restriction on the optical depth of the medium in the treatment of radiative effects, and C) study of oscillating flows. A comprehensive description of most of the results obtained with the present approach may be found in Ref. 8. Comparisons with other calculations or experimental data are included when possible. The cgs system of units is used throughout.

A. Applicability to Attached and Detached Shock Wave Configurations

For a 50.56° half-angle cone the computations were performed at $M_0 = 5$ with the freestream static conditions given by: $\rho_0 = 0.184 \times 10^{-4}$ g/cm^3 and $p_0 = 0.121 \times 10^5$ dyne/cm^2 which correspond to an altitude of approximately 35 km in the Earth's atmosphere. These static conditions will be used in all computations except those including radiation effects. Two cases were considered: 1) solid surface (without mass injection), and 2) massive gas injection into the shock layer.

The steady-state shock positions for a finite length cone without mass injection obtained from our results as well as for an infinite length cone obtained from Ref. 17 are presented in Fig. 3. In the region of conical flow ($r < 60\Delta r$, cone surface extends to $65\Delta r$) the shock angles differ by about 2°. This may be caused by an effective bluntness of the body that forces the shock to move further out than its ideal sharp cone position. The bluntness results from the combination of "artificial viscosity" with large angular gradients near the vertex. In computations with uniform angular increments throughout the field excellent angular resolution near the vertex was attained and the shock angle computed with our method for the finite cone coincided with that tabulated for the infinite cone to within a fraction of a degree. Unfortunately, as mentioned in Sec. III.B, such a nonuniform mesh required inappropriately small time increments which severely distorted results away from the vertex and the technique had to be abandoned.

As Fig. 3 shows, the region of conical flow terminates past about $r = 60\Delta r$ where the influence of the corner is felt. This means that the corner affects the flow in the upstream direction, which should not happen in supersonic flow. The effect is caused by the small dissipative terms in the finite-difference equations.

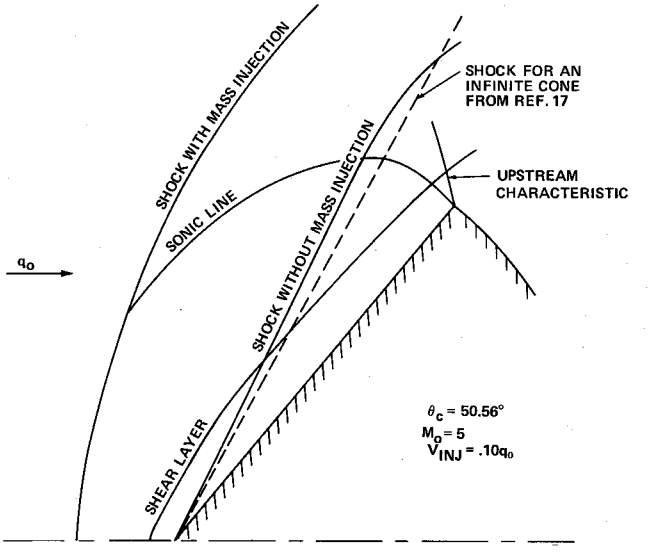

Fig. 3 Flow over a 50.56° half-angle cone.

Included in Fig. 3 is also the effect of large mass injection represented by the curved shock with the sonic line and an estimate of the position of the shear surface. We observe that now the shock is detached; from previous studies we know that the shock layer is divided into inviscid outer and inner layers separated by a viscous shear surface. The oncoming stream effectively sees the blunt shape defined by the thin shear surface. The boundary conditions pertinent to this case are described in detail in Ref. 8.

The location of the shear surface is obtained from pressure profiles[8] that exhibit a shallow minimum between the shock and cone surface; the position of the shear layer is estimated as the locus of points inside the shock layer with maximum pressure gradient. This estimate is suggested by the finding of Wallace and Kemp[18] that, in cases when an analytic solution is possible, matching of pressure on both sides of the contact surface leaves a discontinuity in pressure gradient. The correctness of the preceding interpretation is confirmed by an examination of the direction field of velocity vectors which are tangent to the shear surface.

In order to illustrate how the present method distinguishes between the attached and detached shock configuration, we have prepared Fig. 4. The two curves in that figure represent the pressure variation along the axis-surface streamline for the 50.56° and 90° half-angle cones. We see that for the attached shock configuration the pressure remains at its freestream value along the axis to within a few mesh points of the vertex and then is perturbed slightly. Across the vertex the pressure jumps to almost 90% of its correct value behind the attached shock and continues to approach the correct value some distance away from the vertex. In view of the fact that there is only one angular step between the axis and the cone surface at the vertex and for some distance away from the vertex there are no mesh points between the shock and cone surfaces,[8] such performance of the numerical scheme is

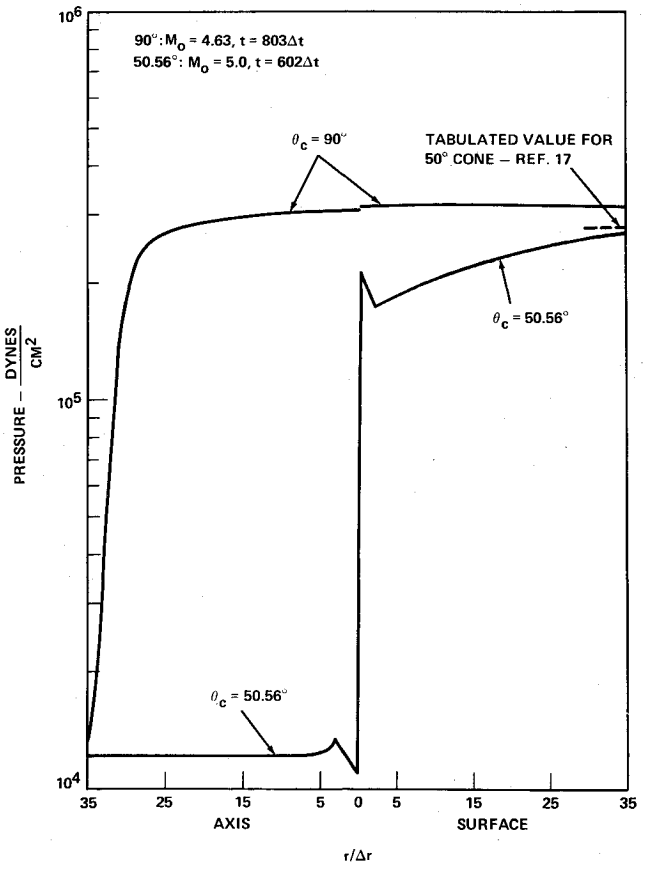

Fig. 4 Pressure along axis-surface streamline for 50.56° and 90° half-angle cones.

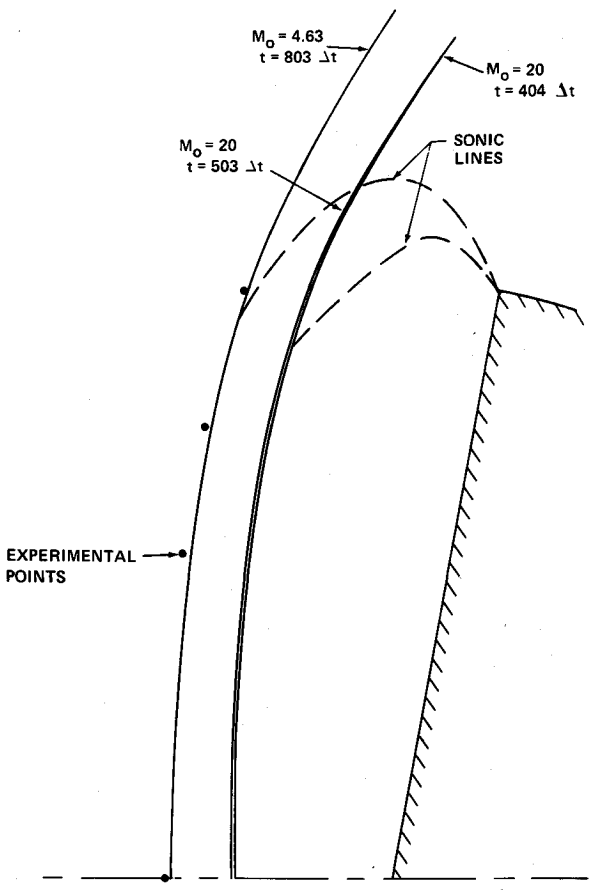

Fig. 5 Shock shapes for a 79.83° half-angle cone.

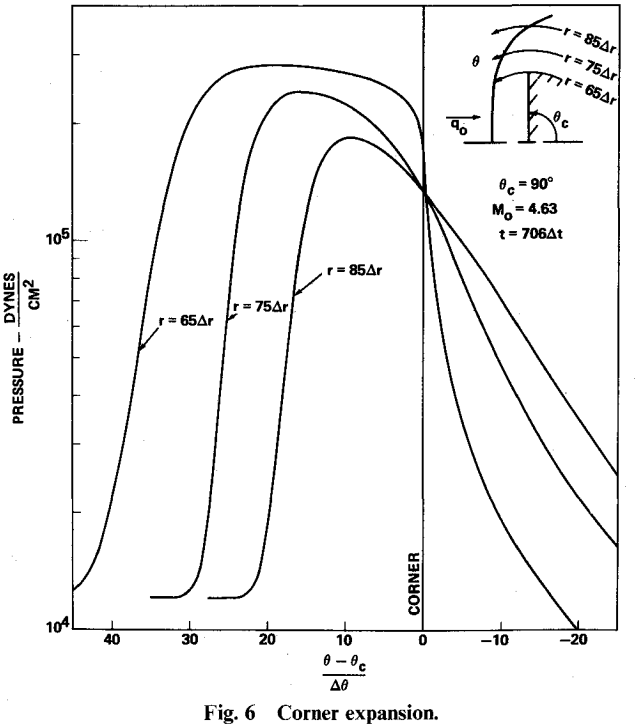

Fig. 6 Corner expansion.

quite good. A more elaborate structure of the mesh near the vertex would improve the accuracy and resolution considerably.

One such possible structure could consist of a somewhat finer angular mesh near the vertex combined with the employment of different time increments Δt in regions of different $\Delta\theta$. Then each time advance would be followed by an appropriate interpolation (possibly extrapolation in some regions) procedure set up to adjust all parts of the field to the same time level prior to next advance.

For the 90° half-angle cone (flat face) the pressure along the axis (stagnation streamline) increases smoothly (with a barely perceptible jump at the singularity of the coordinate system) and monotonically towards the surface.

The steady-state shock positions and sonic lines for a 79.83° half-angle cone at $M_0 = 4.63$ and $M_0 = 20$ are shown in Fig. 5 together with experimental points of Campbell and Howell.[19] Agreement between the numerical computations and experimental results is excellent throughout the shock layer because of the large number of grid points between the shock and the body surface that allows the gradients in this region to be satisfactorily resolved. Because of the higher compression in the shock layer, the shock at $M_0 = 20$ is located significantly closer to the body than at $M_0 = 4.63$. For both Mach numbers, the sonic line is a smooth curve emanating from the corner and intersecting the shock at an acute angle. Thus the present treatment of the corner as a triple-valued point improves on previous corner treatments as a single-valued point[3,4] where the sonic line was found to intersect the body about five mesh points behind the corner. As predicted in Ref. 20, the intersection of the sonic line with the shock moves closer to the axis as the Mach number is increased. The shock inclinations at the point of intersection agree well with the values of critical angles obtained from the NACA chart.[21]

Figure 6 shows sample plots of pressure variation on spherical surfaces behind a 90° half-angle cone. There is a rapid but smooth expansion around the corner and the expansion rate diminishes as the distance from the corner increases.

B. Absence of Slab Approximation

Two calculations were performed to study the three-dimensional radiative effects in both detached and attached shock wave configurations. In the first case, hypersonic flow over the 79.83° half-angle cone was computed with $M_0 = 47.2$, $\gamma = 1.2$, at the freestream static conditions of $\rho_0 = 3.909 \times 10^{-6}$ g/cm^3 and $p_0 = 2.915 \times 10^3$ dyne/cm^2 (corresponding to an altitude of approximately 58 km). The cold wall boundary condition was

used and absorptivity was taken to be proportional to the third power of temperature, (obtained from curve fitting the data on p. 192 of Ref. 22), i.e., $\alpha = \alpha_0 \rho T^3/\text{cm}$, where $\alpha_0 = 0.40 \times 10^{-10}$. Such absorptivity combined with temperature and density behind a $M_0 = 47.2$ shock results in an optical thickness that is approximately 0.62/cm, which means that the shock layer is opaque.

The attached shock wave configuration was investigated for the 50.56° half-angle cone with $M_0 = 15$, $\gamma = 1.4$, $\alpha_0 = 10^{-9}$, and freestream conditions of $\rho_0 = 0.184 \times 10^{-4}$ g/cm^3, $p_0 = 0.121 \times 10^5$ dyne/cm^2.

The time history of the temperature profile (represented by the square of the speed of sound) is shown in Fig. 7. This computation began from a steady-state distribution without radiation effects and ended in a steady state with radiative transport. The result shows that the radiative energy loss not only reduces the temperature by a factor of approximately four (thereby reducing opacity nearly tenfold) but also depresses the temperature profile at the surface in accordance with the cold wall boundary condition. Corresponding to the decrease in temperature is an increase in density and a reduction of the shock layer thickness.

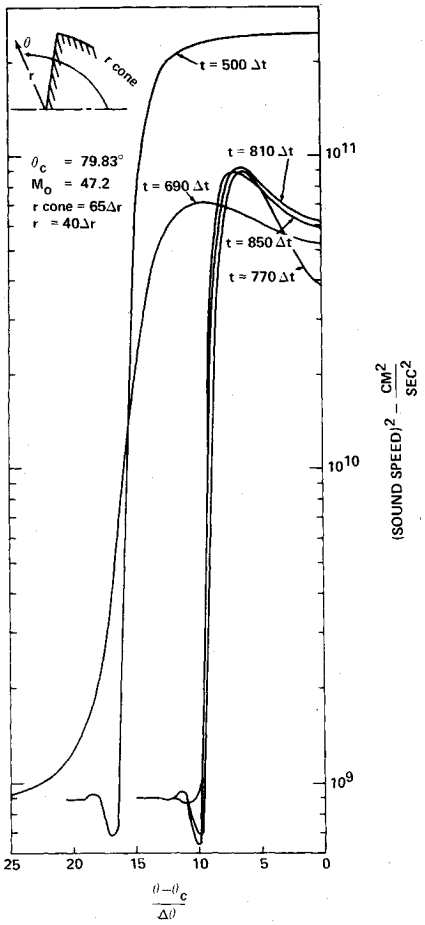

Fig. 7 Effect of radiation in the shock layer.

Computations of radiative effects indicate that one calculation of the radiative field at all points of the mesh (>5000 values) requires approximately 1 hr on the Univac 1108. However, in the calculation of a steady-state solution significant economies in the computer time may be effected because almost everywhere the radiative field (obtained from integration) changes slowly in comparison to the flowfield (obtained from differential equations) and therefore, radiative contribution need be recomputed only every few hundred fluid dynamical time steps. The radiative transfer rate occasionally changes rapidly near the vertex but there are very few points in this region and consequently, frequent computation near $r = 0$ is not time consuming. These two properties are exploited in our program.

The distribution of radiative energy loss across the shock layer at the position of the corner for the 50.56° half-angle cone is shown in Fig. 8. We note the nonsymmetric nature of the shock layer and the presence of a local hot spot at the corner.

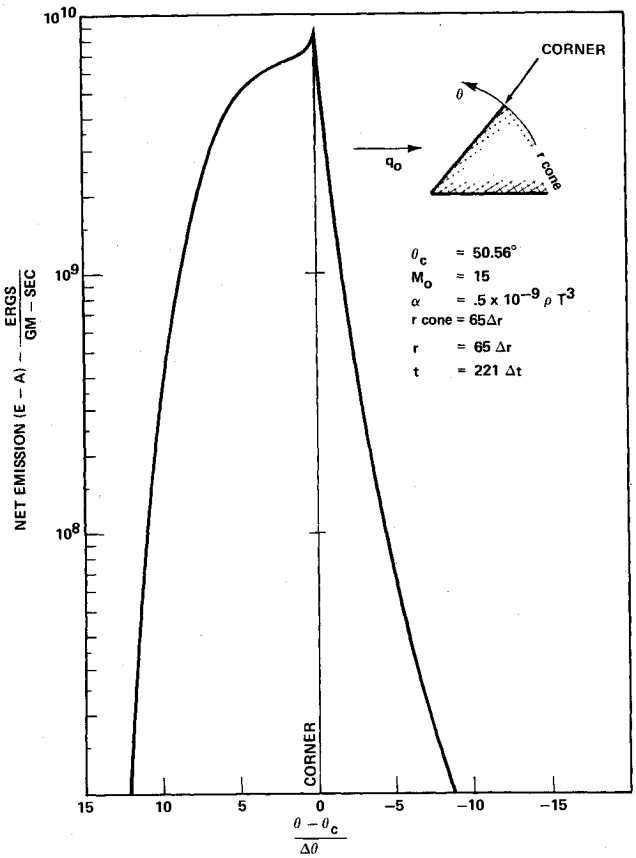

Fig. 8 Shock layer emission.

The results for the 79.83° and 50.56° half-angle cones are compared in Fig. 9, which is a plot of normalized temperatures and radiative energy transfer rates along the surface of the cone from the vertex past the corner. We observe in this figure the

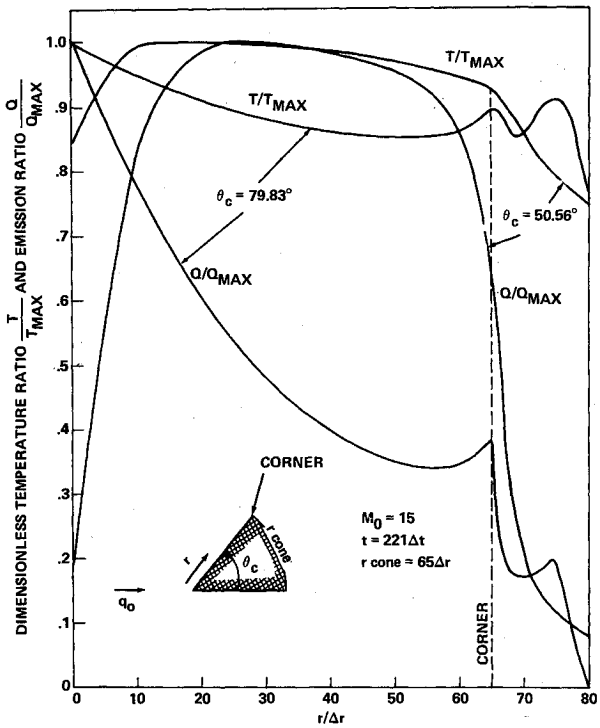

Fig. 9 Temperature and emission along the surface.

qualitatively different behavior of the detached and attached shock wave configurations. In the case of the detached shock wave, the temperature is highest at the vertex, decreases to a minimum near the corner, and increases again to a local maximum at the corner. The second maximum occurs at the point where the ray $\theta = \theta_c$ intersects the shock wave curving behind the corner of a finite length body; it is higher than at the corner because, as Fig. 7 shows, in flows with radiative effects, the temperature is highest immediately behind the shock.

In contrast to the aforementioned behavior of temperature in the case of the detached shock configuration, in the attached shock configuration the temperature increases from the vertex to a maximum along the surface and then decreases again towards the corner and beyond. Such behavior obtains because near the vertex the thin shock layer radiates away energy more efficiently than the thicker layer further downstream. The monotone behavior of temperature near the corner is the vestige of conical similarity of the solution; the ray intersects the shock wave beyond the corner outside of the range of Fig. 9.

The preceding results are three-dimensional effects that cannot be obtained from a slab approximation. Unfortunately, the coordinate system set up in Sec. IV for the evaluation of radiation integrals is such that it precludes the possibility of a direct comparison with the slab approximation. (It is convenient for the specification of rays tangent to the cone.) Such comparison would require a special computer routine which we have not developed in the context of the present investigation.

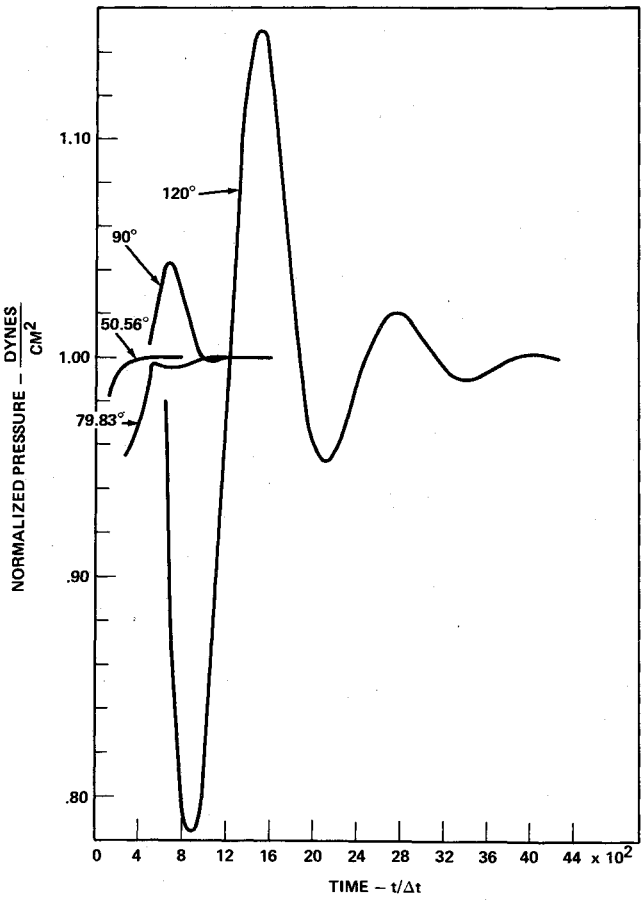

Fig. 10 Pressure transients near vertex for different cone angles.

C. Study of Oscillating Flows

Past studies[7] have shown that the presence of a cavity facing the flow may cause periodic oscillations in the flowfield. Two concave configurations were considered to investigate this phenomenon: 1) conical cavity in a sphere and 2) cylindrical cavity in a cylinder.

The approach of the flowfield to steady state in the case of the 120° half-angle cone is presented in Fig. 10 and compared to similar results for the 50.56°, 79.83°, and 90° half-angle cones. The plots in Fig. 10 represent the time history of normalized pressure on the surface, one mesh point away from the vertex, for each cone angle. The results indicate that the solution corresponding to flow over a spherical body with a conical cavity (120° half-angle cone) undergoes large regular oscillations unlike solutions for the other cone geometries studied. The oscillations appear to be strongly damped and do not persist as was found in Ref. 7. This observation should not be viewed as a contradiction, however, because the geometries considered and methods used in the two analyses are quite different. Rather, it points out a need for further investigations in this direction with a more accurate method.

To study flows over convex shapes with different artificial viscosity and without spurious effects of a nonuniform mesh, computations were made of flow over a hollow cylinder with thin walls, open at one end and closed at the other as shown in Fig. 12. The freestream conditions for these computations are: $M_0 = 10$; $p_0 = 10^4$ dyne/cm^2, $\rho_0 = 10^{-5}$ g/cm^3, the cylinder radius is 37 cm, and wall thickness is zero. Two computations, corresponding to cavity depths of 40 cm and 68 cm, were performed.

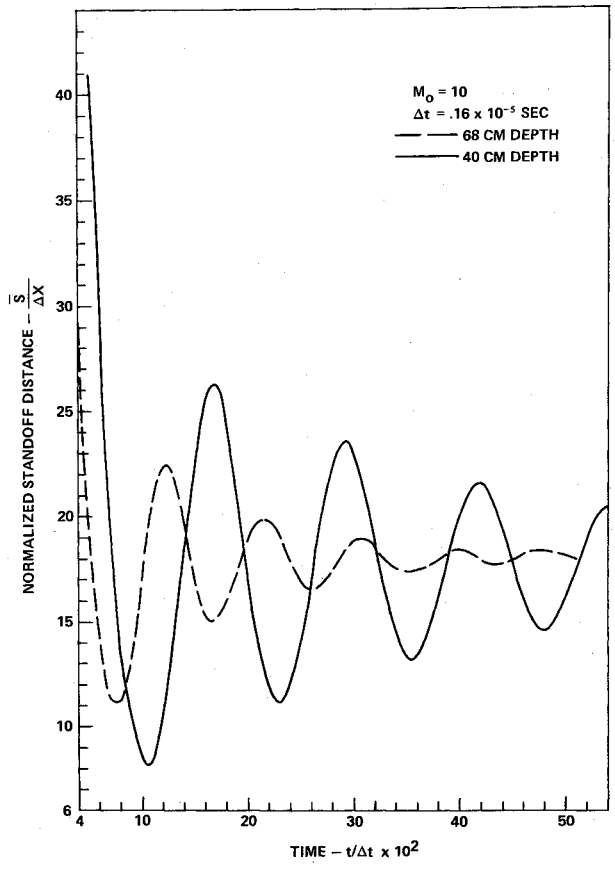

Fig. 11 Shock position on axis vs time.

The time history of the shock position on the axis is shown in Fig. 11. For the initial value problem presented here the shock exhibits damped oscillations before settling down to its steady-state position. Results show that the ratio of the distances from the base of the cavity to the shock equilibrium position is equal to the ratio of the oscillation periods. Thus, for the present geometry, a characteristic length for oscillation is not the tube depth (a geometric property), but the tube base-shock distance (a geometric-thermodynamic property). From simple acoustic theory it is known that a wave moving back and forth in a tube open at one end and closed at the other has a wavelength equal to four times the tube depth; present results yield a measured wavelength equal to about 4.5 times the tube base-shock distance.

The streamline pattern inside the 40 cm deep cavity after 5200 time steps in shown in Fig. 12. The flow in the region near the cavity mouth appears to drive the flow near the base. The driven flow contains a vortex, which changes its position and intensity with time. We conjecture that after a sufficiently long time, the driven flow will form a closed cell and continuously circulate in a clockwise direction. At the time shown, mass from the driven region exits the cylinder, which correlates with a pressure decrease in that region. There was no evidence of the presence of a vortex outside of the cavity at any time.

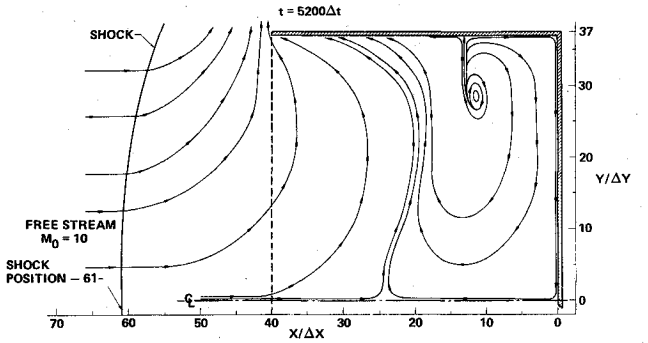

Fig. 12 Flow pattern in the cylindrical cavity.

The cost of obtaining these solutions is approximately 1 hr/1000 time steps on the Univac 1108 computer.

Because of space limitations the preceding is only a summary of the results obtained with our approach. An extensive presentation including discussion of phenomena and observations not mentioned here may be found in Ref. 8. For example, it is concluded that higher-order accurate schemes with much lower dissipation are needed to differentiate between physical and numerical damping.

VI. Conclusions

The numerical unsteady approach set out in this paper has been found to be applicable to the development of a single method for the computation of re-entry flowfields with attached and detached shock waves, It has been demonstrated that the method is useful in the study of mass injection, oscillating flows with shock waves, and of radiation effects without slab approximation or restriction on the optical thickness of the medium.

Future work in this area may proceed in several directions. One is to improve the accuracy and resolution of the results by employing more accurate differencing schemes and/or by devising better numerical procedures for the treatment of surface and internal boundaries, as required for injection effects. It should be noted that the correct specification of boundary conditions for the finite-difference scheme used in the present work is still an open question in numerical analysis. Another direction for future investigations is to perform parametric studies in regions of particular interest, e.g., near the critical cone angle or around the transition from convex to concave body (near $\theta_c = 90°$). Also, when atmospheric entry conditions of particular interest are identified, computations may be performed for the purpose of determining the aerothermodynamic characteristics of entry vehicle shapes described by different cone half-angles. These properties are useful for the study of entry trajectories.

References

[1] Schneider, P. J., Mauer, R. E., and Strapp, M. G., "Two-Dimensional Transpiration Cooling," *Journal of Spacecraft and Rockets*, Vol. 8, No. 2, Feb. 1971, pp. 170–176.

[2] Jarvinen, P. O. and Adams, R. H., "The Effects of Retro-Rockets on the Aerodynamic Characteristics of Conical Aeroshell Planetary Entry Vehicles," AIAA Paper 70-219, New York, 1970.

[3] Bohachevsky, I. O. and Rubin, E. L., "A Direct Method for Computation of Nonequilibrium Flows with Detached Shocks," *AIAA Journal*, Vol. 4, No. 4, April 1966, pp. 600–607.

[4] Bohachevsky, I. O. and Mates, R. E., "A Direct Method for Calculation of the Flow about an Axisymmetric Blunt Body at Angle of Attack," *AIAA Journal*, Vol. 4, No. 5, May 1966, pp. 775–782

[5] Crocco, L., "A Suggestion for the Numerical Solution of the Steady Navier-Stokes Equations," *AIAA Journal*, Vol. 3, No. 10, Oct. 1965, pp. 1824–1832.

[6] Godunov, S. K., Zabordin, A. O., and Prokopov, G. P., "A Finite Difference Scheme for Two-Dimensional Unsteady Flow with a Detached Shock Wave," *Zhurnal Vychyslitelnoi Mat. i Mat. Fiziki*. Vol. 1, No. 6, 1961, pp. 1020–1050; also transl. by Cornell Aeronautical Lab., Buffalo, N. Y.

[7] Bastianon, R., "Steady and Unsteady Solution of the Flow Field Over Concave Bodies in Supersonic Free Stream," AIAA Paper 68-946, El Centro, Calif., 1968.

[8] Bohachevsky, I. O. and Kostoff, R. N., "Supersonic Flow Over Convex and Concave Shapes with Radiation and Ablation Effects," TM71-1013-5, Aug. 2, 1971, Belcomm Inc., Washington, D.C.

[9] Zeldovich, U. B. and Raizer, Y. P., *Physics of Shock Waves and High-Temperature Hydrodynamic Phenomena*, Vol. 1, Academic Press, New York, 1966, Chap. 3.

[10] Lax, P. D., "Weak Solutions of Nonlinear Hyperbolic Equations and their Numerical Computation," *Communications on Pure and Applied Mathematics*, Vol. 7, No. 2, 1954, pp. 159–193.

[11] Richtmyer, R. D. and Morton, K. W., *Difference Methods for Initial Value Problems*, 2nd ed., Interscience Publishers, New York, 1967, p. 300.

[12] Lax, P. and Wendroff, B., "Systems of Conservation Laws," *Communications on Pure and Applied Mathematics*, Vol. 13, No. 2, 1960, pp. 217–237.

[13] Rusanov, V. V., "Finite Difference Schemes of Third Order Accuracy for Continuous Computation of Discontinuous Solutions," AN USSR Preprint, 1967, Inst. of Applied Mathematics; also *Soviet Math. Dokl.*, Vol. 9, No. 3, 1968.

[14] Jackomis, W. N. and Zumwalt, G. W., "Transient Flow Field Analysis of a Plane Blast Wave Intercepting a Stationary Cone at Zero Angle of Attack," Sandia Corp. Rept. SC-DC-66-1329, Aug. 1965, Albuquerque, N. Mex.

[15] Courant, R., Friedrichs, K. O., and Lewy, H., "Über die Partiellen Differenzengleichungen der Mathematischen Physik," *Mathematische Annalen*, Vol. 100, No. 1, 1928, p. 32.

[16] Anderson, J. D., Jr., "An Engineering Survey of Radiating Shock Layers," *AIAA Journal*, Vol. 7, No. 9, September 1969, pp. 1665–1675.

[17] Sims, J. L., *Tables for Supersonic Flow Around Right Circular Cones at Zero Angle of Attack*, NASA SP-3004, 1964.

[18] Wallace, J. and Kemp, N. H., "Similarity Solutions to the Massive Blowing Problems," *AIAA Journal*, Vol. 7, No. 8, Aug. 1969, pp. 1517–1523.

[19] Campbell, J. F. and Howell, D. F., "Supersonic Aerodynamics of Large-Angle Cones," TN-D-4719, Aug. 1968, NASA.

[20] Hayes, W. and Probstein, R., *Hypersonic Flow Theory*, Vol. 1, 2nd ed., Academic Press, New York, 1966, p. 395.

[21] Ames Research Staff, "Equations, Tables and Charts for Compressible Flow," Rept. 1135, 1953, NACA.

[22] Penner, S. S. and Olfe, D. B., *Radiation and Reentry*, Academic Press, New York, 1968, p. 192.